Cationic Lipid-Based Formulations for Encapsulation and Delivery of Anti-*EFG1* 2'*O*MethylRNA Oligomer

Daniela Araújo
University of Minho School of Engineering: Universidade do Minho Escola de Engenharia
Ricardo Gaspar
International Iberian Nanotechnology Laboratory
Dalila Mil-Homens
University of Lisbon: Universidade de Lisboa
Mariana Henrqiques
University of Minho School of Engineering: Universidade do Minho Escola de Engenharia
Bruno Silva
INL: International Iberian Nanotechnology Laboratory
Sónia Silva (sonia.silva@iniav.pt)
INIAV: Instituto Nacional de Investigacao Agraria e Veterinaria

Research

Keywords: Candida albicans, filamentation, nucleic acid mimics, non-viral vectors, lipoplexes carriers.

Posted Date: October 27th, 2021

DOI: https://doi.org/10.21203/rs.3.rs-1004349/v1

Abstract

Background: The effective protection and delivery of antisense oligomers to its site of action is a challenge without an optimal strategy. Some of the most promising approaches encompass the complexation of nucleic acids, which are anionic, with liposomes of fixed or ionizable cationic charge. Thus, the main purpose of this work was to study the complexation of cationic liposomes with anti-*EFG1* 2'*O*Me oligomers and evaluate the complex efficacy to control *Candida albicans* filamentation *in vitro* and *in vivo* using a *Galleria mellonella* model.

Results: To accomplish this, cationic 1,2-dioleoyl-3-trimethylammoniumpropane (DOTAP) was mixed with three different neutral lipids dioleoylphosphocholine (DOPC), dioleoylphosphatidylethanolamine (DOPE) and monoolein (MO) and used as delivery vectors. Fluorescence Cross Correlation Spectroscopy measurements revealed a high association between antisense oligomers (ASO) and cationic liposomes confirming the formation of lipoplexes. *In vitro*, all cationic liposome-ASO complexes were able to release the anti-*EFG1* 2'*O*Me oligomers and consequently inhibit *C. albicans* filamentation up to 60 % after 72 h. *In vivo*, from all formulations the DOTAP/DOPC 80/20 ρ_{chg}=3 formulation proved to be the most effective, enhancing the *G. mellonella* survival by 40% within 48 h and by 25% after 72 h of infection.

Conclusions: In this sense, our findings show that DOTAP-based lipoplexes are very good candidates for nano-carriers of anti-*EFG1* 2'OMe oligomers.

Background

Fungal diseases have emerged as a significant cause of morbidity and mortality, especially among immunocompromised patients (1). The clinical *Candida albicans* infection is responsible for 70-90 % of human fungal infections with a mortality rate up to 40 % (2–5). The pathogenicity of *C. albicans* is supported by a series of virulence factors, one of the most alarming being its ability to switch from yeast to filamentous forms, which enhances human body tissue invasiveness and helps to escape the host's immune system (6,7). *EFG1* plays a central role in the regulation of the filamentous morphology and in the virulence of *C. albicans* (6,8,9).

As a consequence of the rising of *C. albicans* multi-resistance to antifungal agents, new treatment strategies with novel mechanisms of action and enhanced therapeutic potential are urgently needed. Antisense oligomers (ASOs) hold great promise for the treatment of infectious diseases and particularly for the control of *C. albicans* virulence genes (10–14). Recently, we demonstrated the ability of the anti-*EFG1* 2'OMethylRNA oligomer to control *EFG1* gene expression and Efg1p protein translation, preventing *in vitro C. albicans* filamentation (15).

Despite these advances, the delivery of ASO to their site of action remains a key challenge and it appears that finding delivery vehicles is generally problematic (16). Recently, various non-viral vectors have been engineered for improved gene and drug delivery (17–19). Some of the most promising strategies for delivery of nucleic acids encompass complexation of nucleic acids, which are anionic, with liposomes of

fixed or ionizable cationic charge (20–24). Due to attractive electrostatic interactions between cationic liposomes and nucleic acids, new nanostructured complexes, often referred to by lipoplexes, tend to be formed (25–28). Besides facilitating the formation of nanostructured particles with high encapsulation efficiency, the cationic charge of liposomes also favours attractive interactions with cellular and endosomal membranes, improving cellular uptake and endosomal release (22,29,30). Typically, cationic liposomes used in nucleic acid delivery are composed by at least two lipid components: a cationic lipid (e.g., 1,2-dioleoyl-3-trimethylammoniumpropane (DOTAP)) and a neutral or zwitterionic lipid, such as dioleoylphosphocholine (DOPC). The incorporation of the neutral lipid allows adjusting the amount of positive charge per liposome area (i.e. membrane charge density - σ_M) (29,30). Simultaneously, some neutral lipids such as dioleoylphosphatidylethanolamine (DOPE) and monoolein (MO) improve the lipoplexes' fusogenic properties, helping the lipid-nucleic acid complex fuse with endosomal membranes (18,31,32). Both the ability to modulate σ_M and fusogenicity are known to influence the transfection efficiency (29,30).

To have a broader scope at the liposome compositional level, we use the generic cationic lipid DOTAP, combined with three different neutral lipids DOPC, DOPE and MO. Whereas combined with DOTAP, DOPC is known to favour the formation of lamellar-type complexes, DOPE and MO are known to favour the formation of inverted structures depending on their molar fractions. Thus, the main purpose of this work was to study the complexation of cationic liposomes with anti-*EFG1* 2'*O*Me oligomers, along with its efficacy to control *C. albicans* filamentation *in vitro* and *in vivo* using a *Galleria mellonella* model.

Overall, we find that cationic liposomes improve the efficiency of anti-*EFG1* 2'OMethylRNA after 48h. *In vitro* the most efficient formulations identified were for systems with high cationic lipid content (high σ_M) and high cationic to anionic charge ratio (ρ_{chg}=10). In the *G. mellonellain vivo* model, we find that it is the formulation with lower ρ_{chg} (ρ_{chg}=3) that improves survival the most.

Results And Discussion

The use of ASOs for the treatment of important genetic disorders has emerged as a promising approach (11,12,14,33,34). More recently, this approach has also shown promissory results in the control of *C. albicans* virulence determinants (35). However, ASO penetration into *Candida* cells can be limited by the cell wall envelope which is composed of several layers surrounding the cytosol (36). Therefore, delivery strategies are needed to ensure that ASO crosses *Candida*'s cell wall and that it also confers protection against degradation by serum proteases and nucleases in the host (37). At the present time, most delivery approaches for gene delivery employ either viral or non-viral vectors (17). Viral vectors show high gene silencing activity, however they present associated risks, including the activation of inflammatory and immune responses in the host (17,38). Some of these problems can be circumvented by employing non-viral vectors, such as cationic lipoplexes (16,18,39,40), which are assemblies that result from the electrostatic complexation between cationic liposomes and negatively charged ASO (31). Lipoplexes tend to have well-ordered hexagonal, cubic bicontinuous or multilamellar structures with the ASO sandwiched

between the bilayers (18). Thus, the main goal of this work was to study the formation of cationic lipid-anti-*EFG1* 2'OMe oligomer complexes along with their capability to control *C. albicans* filamentation *in vitro* and *in vivo* way using the *G. mellonella* model. Three different neutral lipids (DOPC, DOPE and MO) combined with DOTAP (cationic lipid) were used, in a composition range where multilamellar structures are expected to be formed.

Lipoplex characterization

To note, cationic and neutral lipids are usually used to form liposomes for gene delivery due to their favourable interactions with negatively charged RNA or DNA and with cell membranes (31). Moreover, the neutral lipids are usually included as 'helper' lipids to enhance the transfection activity and nanoparticle stability (17,18,40). Lipoplexes can adopt different structures (e.g. lamellar) depending on the type of lipids used and number of cationic and neutral charges in its composition (Table 1). The association between *n* ASO and *m* cationic liposomes (CLs) to form a *m*CL.*n*ASO complex can be considered according to the following equilibrium:

$$m\text{CL} + n\text{ASO} \rightleftharpoons m\text{CL}.n\text{ASO} \qquad (3)$$

For simplicity we will refer to *m*CL.*n*ASO complexes simply as CL-ASO complexes or lipoplexes. If ASO and CLs are labelled with two different fluorescent dyes (in this case, ASO with Tye-563 – red – and CLs with Atto-488 – green), this association can be followed with Dual-color Fluorescence Cross-Correlation Spectroscopy (FCCS) (41–43).

For such scenario, if one neglects cross-talk between the two fluorescent channels, the amplitudes of the autocorrelation curves of the individual green and red channels (G_G and G_R, respectively) and the amplitude of the cross-correlation curve between them (G_X) are given by Eqs 4 (42,43):

$$G_G(0)=\frac{(m\cdot q_{CL})^2\cdot C_{CL\text{-}ASO}+C_{CLf}}{V_G(m\cdot q_{CL}\cdot C_{CL\text{-}ASO}+C_{CLf})^2} \quad (4a)$$

$$G_R(0)=\frac{(n\cdot q_{ASO})^2\cdot C_{CL\text{-}ASO}+C_{ASOf}}{V_R(n\cdot q_{ASO}\cdot C_{CL\text{-}ASO}+C_{ASOf})^2} \quad (4b)$$

$$G_X(0)=\frac{m\cdot q_{CL}\cdot n\cdot q_{ASO}\cdot C_{CL\text{-}ASO}}{V_X(n\cdot q_{ASO}\cdot C_{CL\text{-}ASO}+C_{ASOf})\cdot(m\cdot q_{CL}\cdot C_{CL\text{-}ASO}+C_{CLf})} \quad (4c)$$

Here q_{CL} and q_{ASO} are factors accounting for quenching (q_i <1) or FRET (q_i >1) of the molecular brightness of complexed liposomes and ASO in the green and red detectors, respectively. V_G and V_R are the effective volumes in the green and red channels and V_X is the volume overlap between them. C_{CL}, C_{ASO} and $C_{CL\text{-}ASO}$ are the concentrations of CLs, ASO and CL-ASO in those effective volumes, respectively. Importantly, while G_G and G_R are concerned with the dynamics and relative concentrations of all the species that are labelled green or red, respectively, G_X is concerned with the dynamics and relative concentrations of species that carry both dyes simultaneously (i.e. CL-ASO complexes). Hence, FCCS is an excellent probe to monitor the association between ASO and liposomes.

While, experimentally, we try to minimize cross-talk between the two channels, the equations are still very complicated to solve since there are many experimental unknowns difficult to determine. This is in contrast with more conventional lipid-DNA lipoplexes, where the large DNA length and charge ensure a practically complete DNA encapsulation for ρ_{chg} >1, and complete cationic liposome consumption for ρ_{chg}<1, allowing a simplification of some of the terms in eqs. 4 (43). For ASO these assumptions cannot be entirely met. However, even though Eqs. 4 cannot be used to determine *m* and *n* and overall encapsulation efficiency, FCCS can still provide important information, especially if the experimental results from the cationic liposome formulations are compared with a control system where complexation is not expected to occur. Figure 1 shows the auto- and cross-correlation curves for the different cationic liposome-ASO formulations at ρ_{chg}=3 and high cationic lipid content (80/20). In addition, pure DOPC liposomes incubated with ASO used as a control system is also shown (Figure 1 D). Since DOPC liposomes are net-neutral, no significant interactions with ASO leading to the formation of lipoplexes are expected. The concentration of DOPC used was equivalent to the concentration of DOTAP used for ρ_{chg}=3.

Figure 1 shows high G_X amplitudes, comparable to both G_G, and G_R, for the cationic liposome formulations. In contrast, the DOPC sample shows a much reduced amplitude of G_X, whose value is ca. 0.4 (this value is not zero most likely because of cross-talk of the green fluorescence of the liposomes to the red channel). Through eq. 4c it is possible to see that the larger G_X amplitudes (beyond cross-talk) observed for the cationic formulations is indicative of association between ASO and cationic liposomes, and hence, the formation of lipoplexes. Another strong indication for the formation of lipoplexes can be extracted from the G_R amplitudes, which are related with the ASO. In the DOPC formulations the amplitude of G_R is practically zero, indicating a very large number of independent ASO molecules diffusing in solution. This is what would be expected if no lipoplex formation occurs. In contrast, in the cationic liposome formulations the amplitude of G_R is finite, comparable to the amplitudes of G_G and G_X, thus indicating a much smaller number of independent ASO species in solution. This is what would be expected if the ASO are complexed with cationic liposomes. Details on the differences in amplitudes of G_R, G_G and G_X for the different cationic liposome formulations are difficult to interpret due to the large number of unknowns in eqs 4, but overall, even without the possibility to determine *m*, *n* and encapsulation efficiency, the formation of lipoplexes is confirmed. These results are also in agreement with what is found for other systems of small oligonucleotides with cationic liposomes and cationic surfactants, in which lipoplex formation is observed for different ρ_{chg} (25,44,45).

The amplitudes of G_X are very high in the case of cationic liposome formulations, but very low for DOPC, indicating the formation of CL-ASO complexes in the former but not on the latter. The very low amplitude of G_R for DOPC also suggests that a very high amount of ASO is diffusing independently (thus not complexed), whereas the high amplitudes of G_R for the cationic liposome formulations suggests the opposite.

In addition to the quantitative information regarding the association between ASO and cationic liposomes, fitting of the cross-correlation curves also provides the size of the lipoplexes. FCCS can be expected to provide more accurate size estimates for a polydisperse solution than, for example, Dynamic Light Scattering (DLS) (43). For DOTAP/DOPC formulations, one observed a radius ranging from 25-35 nm, with lipoplexes prepared at ρ_{chg}=3 slightly smaller to those prepared at ρ_{chg}=10 (Table S1). For DOTAP/DOPE formulations, a similar trend was observed with particles ranging from 25-40 nm, and with a slight smaller size observed for formulations prepared are ρ_{chg}=3 being slightly smaller (Table S1). Finally, DOTAP/MO formulations appeared to produce the smallest particles with sizes ranging from 18-25 nm (Table S1), were those containing more cationic lipid were shown to be slightly larger, independent to the ρ_{chg}.

In vitro effects of lipoplexes on C. albicans filamentation

The anti-*EFG1* 2'OMe oligomer cationic lipid-based formulations efficacy was evaluated in terms of its ability for controlling *C. albicans* filamentation (Figure 2). Noteworthy, all formulations were able to

control *C. albicans* filamentation, although to different extents. It is also important to highlight that in general the reduction on *C. albicans* filamentation increases over time for all lipoplexes, with a similar trend observed for free ASO.

It should be noted that the encapsulation of anti-*EFG1* 2'OMe oligomer with DOTAP/DOPC liposomes (Figure 2 A) shows a slight improvement in the *C. albicans* filamentation reduction after 48 h and 72 h when compared to free-ASO (P-value>0.05). Figure 2 B presents the data related to treatment of *C. albicans* cells with DOTAP/DOPE lipoplexes. All the DOTAP/DOPE formulations feature a similar or superior efficacy to that of free-ASO. All DOTAP/MO lipoplexes tested improved the efficacy in comparison to free-ASO, especially at 48 h (P-value<0.05). The DOTAP/MO 80/20 ρ_{chg}=10 lipoplexes, typically with a lamellar structure, showed the highest ability to control *C. albicans* filamentation. This could be related with the fusogenicity of MO which may facilitate the fusion of the lipoplex membranes with endosomal membranes and consequently facilitate endosomal release (46,47). Both effects are thought to facilitate the fusion of the lipoplex membranes with endosomal membranes and consequently facilitate endosomal release (47,48). Overall, these results are in agreement with the findings for an analogous system composed by DOTAP/MO but encapsulating siRNA (46).

Figure 3 (A and B) shows that all lipoplexes tested were not only able to decrease the number of *C. albicans* cells as filaments but also to reduce their filament's length up to 40-70 % (P-value>0.05).

In vivo effects of lipoplexes on G. mellonella survival

The invertebrate model of *G. mellonella* was used to test *in vivo* the efficacy of lipoplexes carrying anti-*EFG1* 2'OMe ASO. The lipoplexes tested *in vivo* were DOTAP/DOPC 80/20 ρ_{chg}=3, DOTAP/DOPC 80/20 ρ_{chg}=10, DOTAP/DOPE 80/20 ρ_{chg}=10 and DOTAP/MO 80/20 ρ_{chg}=10 formulations. Two of which were selected based on the *in vitro* data: DOTAP/MO 80/20 ρ_{chg}=10 with the best and the DOTAP/DOPC 80/20 ρ_{chg}=3 due to its lower efficacy *in vitro*. Additionally, were also chose the formulaltions DOTAP/DOPC 80/20 ρ_{chg}=10 and DOTAP/DOPE 80/20 ρ_{chg}=10.

The toxicity effects of the anti-*EFG1* 2'OMe ASO cationic lipid-based formulations was evaluated. Notably, the results in Figure 4 A show the absence of toxicity for all lipoplexes tested.

To study the effect of anti-*EFG1* 2'OMe ASO lipid-based formulations *in vivo*, *G. mellonella* larvae infected with a lethal dose of *C. albicans* were treated with the anti-*EFG1* 2'OMe oligomer cationic lipid-based formulations. The treatment with a single-dose of each lipoplex enhanced the survival of larvae over 72 h (Figure 5). To note, that DOTAP/DOPC 80/20 ρ_{chg}=3 presented the best performance, enhancing the *G. mellonella* survival by 19 % (at 24 h and 48 h) and by 14 % (at 72 h) (P-value<0.05). In contrast, DOTAP/DOPC 80/20 ρ_{chg}=10 revealed to be the less efficient. Therefore, in contrast to the *in vitro* findings, *in vivo* the ρ_{chg} seems to influence the DOTAP/DOPC 80/20 lipoplexes efficacy, with the ρ_{chg}=3 formulation presenting a higher increase on larvae survival than ρ_{chg}=10.

It was also observed that DOTAP/DOPE 80/20 ρ_{chg}=10 (Figure 5 B) increased the *G. mellonella* survival over 72 h (P-value<0.05), however to a slight extension when compared to the performance of DOTAP/DOPC 80/20 ρ_{chg}=3. Although the *G. mellonella* survival increased after 24 h and 48 h of treatment with the DOTAP/MO 80/20 ρ_{chg}=10 lipoplex in comparison to the untreated larvae, no statistic differences were observed after 72 h (Figure 5 C) (P-value>0.05).

The invasiveness progression of *C. albicans* into the fatty body of larvae is represented in Figure 5D. Figure 5A confirms that *C. albicans* cells tend to locate mainly in the *G. mellonella* digestive system (49). Moreover, an extensive progression is evident over the 48 h of infection and is predominantly composed of the filamentous form, which are more invasive to tissues than yeast cells and provides a mechanism for evasion of the host's defence mechanism (50). The treatment of *G. mellonella* with all the lipoplex formulations resulted in a lower quantity of *C. albicans* cells on the larvae digestive system with a significant reduction on the number of filaments (Figure 5 B-D).

To mimic a more real clinical application (51,52), the effect of double-dose administration of the DOTAP/DOPC 80/20 ρ_{chg}=3 formulation (the lipoplex with the best efficacy in the single-dose studies) was analysed. To note, the double-dose administration of DOTAP/DOPC 80/20 ρ_{chg}=3 enhances the *G. mellonella* survival by a factor of ca. 1.5 when comparing to the single-dose administration, increasing the larvae survival by 40 % after 48 h and by 25 % after 72 h of treatment (P-value<0.005) (Figure 6 A). It is important to point out that the double-dose administration also potentiates the effect of free-ASO by a factor of ca. 1 (a survival increase by 18 % after 24 h and 13 % after 72 h of infection (P-value<0.05)). Moreover, the fatty bodies histological analysis confirms the decrease on *C. albicans* cells filamentation when treated with the DOTAP/DOPC 80/20 ρ_{chg}=3 lipoplex (Figure 6 B).

Effectively, the survival rate of *G. mellonella* when treated with the anti-*EFG1* 2'OMe ASO cationic lipid-based formulations was significantly higher than when treated with free-ASO. This evidence confirms the importance of the encapsulation for protecting ASO against the degradation by serum proteases and nucleases.

Lipoplexes have been studied for the delivery of nucleic acids *in vitro* and in clinical trials (53) often with promising results (21). Here we show that lipoplexes also successfully encapsulate and deliver anti-*EFG1* 2'OMe oligomers into *C. albicans* cells, helping to control filamentation and improving the survival of infected larvae model.

This study demonstrated the successful delivery of anti-*EFG1* 2'OMe ASO encapsulated in cationic lipid-based formulations, providing valuable information for further assays. Although, DOTAP/DOPC 80/20 ρ_{chg}=3 had a lower efficacy to inhibit filamentation *in vitro*, it was revealed to be the best formulation *in vivo* to control *C. albicans* virulence. Therefore, the DOTAP/DOPC 80/20 ρ_{chg}=3 formulation has the potential to improve nanodrug administration for *C. albicans* species.

Conclusion

The delivery of pharmaceuticals to its site of action is a challenge and there is not an optimal delivery strategy. In the case of antisense oligonucleotides, it is important to protect them against innate immune system. In this sense, our findings confirm that lipoplexes based on DOTAP as cationic lipid can be used as possible carriers of anti-*EFG1* 2'OMe ASO. Particularly, the DOTAP/DOPC 80/20 ρ_{chg}=3 formulation revealed to be the most efficient formulation to improve nanodrug administration for *C. albicans* species.

Materials And Methods

Materials

The anti-*EFG1* 2'*O*Me oligomer with sequence 5'-mG mG mC mA TACCGTTA mU mU mG mU-3' (m- 2'-*O*Me), was designed based on second generation of nucleic acid mimics and synthesized according to the suppliers' own specifications at EXIQON, as described in previous works (15,35). A stock of ASO at 4 µM was prepared in sterile ultrapure water and stored at -20 °C for later use.

Lipids DOTAP, DOPC, and DOPE dissolved in chloroform, were purchased from the Avanti Polar Lipids (USA). MO was purchased from Nu-Chek Prep (Elysian, MN, USA). All lipids were used as received.

Preparation of liposomes and lipoplexes

Liposomes were prepared with different lipid compositions and membrane charge densities σ_M, as described in Table 1. In order to achieve this, cationic DOTAP was mixed together with different helper lipids DOPC, DOPE or MO at different molar ratios. Lipid stocks dissolved in chloroform were mixed in the desired ratios and fluorescently labelled by adding Atto-488 DHPE to the lipid solution (0.1% molar ratio). The resulting mixture was dried using a constant nitrogen gas stream, and then placed in vacuum overnight. The lipid film was resuspended in ultrapure nuclease free Milli-Q water. The suspensions were vortexed and sonicated using a tip sonicator for 1 min, with 10 % amplitude and 50 % duty cycle using a Branson Digital Sonifier 250 Model. The size of the liposome solutions reported were determined with DLS using a SZ-100 device from Horiba, measuring scattering at a detection angle of 90° and 173°.

Table 1. Lipid compositions of lipoplexes.

Cationic Lipid	Helper Lipid	Cationic/helper lipid molar %	Lipoplex cationic:anionic charge ratio (ρ_{chg})	Typical lipoplex structure
DOTAP	DOPC	80/20	3	Lamellar (65)
			10	
	DOPE	80/20	3	Lamellar (66)
			10	
	MO	80/20	3	Lamellar (46)
			10	

The different cationic liposomal formulations used along with their respective lipid membrane compositions, cationic-to-anionic charge ratios and the expected lipoplex nanostructure.

For lipoplex formation, equal volumes of liposomes and ASO solutions previously diluted to the desired concentrations were mixed to a final anti-*EFG1* 2'OMe oligomer concentration of 40 nM. The resulting mixture was promptly vortexed for 30 s and left at least 30 min under stirring conditions. The formed complexes were stored at 4 °C. Lipoplexes were prepared with a ρ_{chg} of 3 and 10. The ρ_{chg} is calculated as the total number of positive charges (from the number of DOTAP molecules) divided by the total number of negative charges (from the number and valency of ASO molecules).

Lipoplex characterization

FCCS constitutes an ideal technique to quantify the colocalization between different species at the nanoscale (54–57), including protein-protein interactions (42,58), oligonucleotide-protein interactions (59,60), and cationic liposome-DNA complex formation (41,43) and DNA release (61).

FCCS measurements were performed on a Zeiss LSM 780-NLO confocal microscope (Carl Zeiss AG, Jena, Germany) with a Zeiss C-Apochromat 40×/1.2 W objective, as described in Bacia and Schwille (55) and Gómez-Varela et al (43). High-quality coverslips with a thickness of 170 μm ± 5 μm required for reliable FCCS measurements were used. The coverslip was placed directly on the immersion water drop on top of the immersion water objective with a correction collar.

Atto-488 fluorescence was excited using the 488 nm line of the Argon (Ar) laser and Tye-563 was excited using the 561 nm diode-pumped solid state (DPSS) laser. The main dichroic beam splitter used to separate the incident and the emitted light was MBS 488/561/633.

For the experiments here shown, the fluorescence collection wavelength range was determined by the smart set-up algorithm of the confocal microscope, obtaining in this manner the optimal spectral

detection windows for both FCCS channels with minimal cross-talk derived from the fluorophore spectral emission profiles. The detection range used was 499 - 551 nm for the green channel and 578 – 692 nm for the red channel. Laser powers were adjusted to minimize false-contribution to the cross-correlation by keeping the laser excitation of the green species relatively low compared to the red species (55). Series of sixty consecutive fluorescence intensity fluctuations measurements were conducted for every sample, each recording of 5 s. The effective green (V_G) and red (V_R) volumes are determined by calibration with probes of known diffusion coefficient. The data was automatically extracted, averaged and fitted using a home-built Matlab 2018b script (43). Sixty autocorrelation and cross-correlation curves obtained from five-second-long measurements each are averaged into single mean auto-correlation and cross-correlation curves. The autocorrelation function reflects the self-similarity of the fluorescent signal over the lag time τ and provides a relationship between the average duration a molecule stays in the confocal volume and the diffusion coefficient *D*. If one assumes free-diffusion in three dimensions, we can represent the autocorrelation function *G* through:

$$G(\tau)=G(0)\left(1+\frac{4D\tau}{\omega^2}\right)^{-1}\left(1+\frac{4D\tau}{w_z^2}\right)^{-1/2}=G(0)\left(1+\frac{\tau}{\tau_D}\right)^{-1}\left(1+\frac{\tau}{\tau_D S^2}\right)^{-1/2} \qquad (1)$$

where, $S = \omega_z/\omega_0$ is the aspect ratio between the axial and lateral radii of the detection volume and τ_D the diffusion time. The diffusion coefficient was subsequently determined according to $D=\omega_0^2 / 4\tau_D$ whereas the species hydrodynamic radius is determined through the Stokes-Einstein relation. Noteworthy, is that Eq. 1 is a simple model that assumes a single particle size.

In vitro effects of the lipoplexes

Microorganism and growth conditions

The *Candida* strain used in this study was the reference *C. albicans* SC5314, belonging to the *Candida* collection of the Biofilm group at the Centre of Biological Engineering and its identity was confirmed using a chromogenic medium, CHROMagar™ *Candida*, through the distinction of colonies' colours and by PCR-based sequencing with specific primers (ITS1 and ITS4) (62).

For all experiments, the yeast strain was subcultured on sabouraud dextrose agar (SDA; Merck, Germany) and incubated for 24 h at 37 ℃. Cells were then inoculated in sabouraud dextrose broth (SDB; Merck, Germany) and incubated overnight at 37 °C, 120 rpm. After incubation, the cell suspensions were centrifuged for 10 min at 3000 g at 4 ℃ and washed twice with phosphate-buffered saline (PBS; pH 7, 0.1 M). Pellets were suspended in 5 ml of Roswell Park Memorial Institute (RPMI; Sigma, St Louis, USA), and the cellular density was adjusted for each experiment using a *Neubauer* chamber (Marienfild, Land-Konicshofem, Germany) to $1x10^6$ cells ml^{-1}.

Effect on C. albicans filamentation

The effect of anti-*EFG1* 2'OMe oligomers released from lipoplexes was evaluated in terms of its ability to reduce *C. albicans* filamentation (15). For that, on 24-well polystyrene microtiter plates (Orange Scientific, Braine- l'Alleud, Belgium) 500 µL of each lipoplex was added to 500 µL of a suspension of *C. albicans* at $1x10^6$ cells mL^{-1}. The solutions were incubated at 37 °C and 120 rpm during 72 h. As control, 500 µL of *C. albicans* cells was incubated with 500 µL of 40 nM of free ASO. The positive control was prepared only with *C. albicans* cells and the negative controls with empty liposomes together with *C. albicans* cells in RPMI. The results were presented as percentage (%) of filamentation reduction, through the following equation:

$$\%\ \text{of filamentation inhibition} = \frac{\%\ \text{filament cells (positive control)} - \%\ \text{filament cells (lipoplex)}}{\%\ \text{filaments cells (positive control)}} \quad (2)$$

In parallel, epifluorescence microscopy images were obtained to confirm the levels of *C. albicans* filamentation inhibition and to determine filament's length. The images were obtained through fluorescence microscopy (Olympus BX51) coupled with a DP71 digital camera and the filter used was DAPI – 360-370/420 (Olympus Portugal SA, Porto, Portugal). *Candida albicans* was stained with 1% (v/v) of calcofluor (Sigma-Aldrich, St. Louis, MO, EUA) for 15 min in dark conditions, centrifuged for 5 min and washed twice with ultra-pure water. The images were acquired with the program FluoView FV100 (Olympus). The filament length was determined using ImageJ plug-in software (Maryland, USA).

In vivo effects of the lipoplexes

Galleria mellonella larvae

The *Galleria mellonella* capillary infection model was used for the *in vivo* studies as described by Mil-Homens et al (63). *Galleria mellonella* larvae were reared on a pollen grain and bee wax diet at 25 °C in the dark and used in a final stage with a weight of approximately 250 mg. The larvae were injected in hemolymph via the hindmost left proleg, previously sanitized with 70 % (v/v) ethanol, using a micro syringe adapted in a micrometer to control the volume of injection (63,64).

The lipoplexes selected to test *in vivo* were the DOTAP/DOPC 80/20 ρ_{chg}=3 and ρ_{chg}=10, the DOTAP/DOPE 80/20 ρ_{chg}=10 and DOTAP/MO 80/20 ρ_{chg}=10.

Toxicity evaluation

To test the *in vivo* toxicity of the selected lipoplexes, a set of 10 *G. mellonella* larvae were injected with 5 µL of each formulation. As control a set of larvae were injected with the same volume of free-ASO

prepared in PBS. Larvae were placed in petri dishes and stored in the dark at 37 °C. Larvae survival was recorded over 72 h and survival curves were constructed.

Galleria mellonella survival

To study the *in vivo* effect of lipoplexes, *G. mellonella* larvae were infected with a lethal dose of *C. albicans* cells ($7x10^7$ cells mL^{-1} in PBS) and randomly allocated to different experimental groups (a set of 10 larvae). The concentration of *C. albicans* to be injected was determined based on *G. mellonella* lethality results after injection with increasing concentrations of yeasts ($7x10^7$ cells mL^{-1} to $2x10^8$ cells mL^{-1}) (data not shown). A set of larvae was injected with a single-dose of each lipoplex (0 h post infection) and another with a double dose of each lipoplex solution (0 h and 12 h post infections). As controls, larvae were treated with free-ASO and only with PBS. Larvae were placed in petri dishes and stored in the dark at 37 °C over 3 days, and consequently, the survival curves were constructed. Caterpillars were considered dead when they displayed no movement in response to touch (63).

Galleria mellonella histological assays

Histological analysis of the fatty body of *G. mellonella* were also performed to evaluate the effect of lipoplexes on *C. albicans*' filamentation. For each condition two larvae were recovered at 24 h and 48 h, to be processed histologically. The fat bodies were removed from larvae through an incision in the midline of the ventral with a scalpel blade, placed in 10% formalin and stored at 4 °C to preserve the structures. The fatty bodies were mounted in paraffin blocks and cut in sections of 4-5 µm which were stained with periodic acid Schiff (PAS) and haematoxylin-eosin (HE). For *C. albicans* cells morphological analysis, sections of fatty bodies stained with PAS were observed under a light microscope and photographed with an OLYMPUS BX51 microscope (Olympus Portugal SA, Porto, Portugal) coupled with a DP71 digital camera to distinguish between yeast and filamentous form.

Statistical analysis

Data are expressed as the mean ± standard deviation (SD) of a least three independent experiments. Results were compared using two-way ANOVA and Tukey's multiple comparisons tests. Kaplan-Meier survival curves were plotted and differences in survival were calculated by using log-rank Mantel-Cox statistical test. All performed with GraphPad Prism 6® (GraphPad Software, San Diego, CA, USA).

Abbreviations

Ar: Argon; ASO: Antisense oligomers; CL: cationic liposome; DLS: Dynamic Light Scattering; DPSS: diode-pumped solid state; DOPC: dioleoylphosphocholine; DOPE: dioleoylphosphatidylethanolamine; DOTAP: 1,2-dioleoyl-3-trimethylammoniumpropane; FCCS: Fluorescence Cross-Correlation Spectroscopy; HE:

haematoxylin-eosin; MO: monoolein; PAS: periodic acid Schiff; PBS: phosphate-buffered saline; RPMI: Roswell Park Memorial Institute; SD: standard deviation; SDA: sabouraud dextrose agar; SDB: sabouraud dextrose broth

Declarations

Acknowledgments

This study was supported by the Portuguese Foundation for Science and Technology (FCT) under the strategic funding of UIDB/04469/2020 unit and BioTecNorte operation (NORTE-01-0145-FEDER-000004) funded by the European Regional Development Fund under the scope of Norte2020 - Programa Operacional Regional do Norte and Daniela Eira Araújo [SFRH/BD/121417/2016] PhD grant. The authors also acknowledge the project funding by the “02/SAICT/2017 – Projetos de Investigação Científica e Desenvolvimento Tecnológico (IC&DT) – POCI-01-0145-FEDER-028893”. This research is also supported by Microfluidic Layer-by-layer Assembly of Cationic Liposome-Nucleic Acid Nanoparticles for Gene Delivery project (032520) co-funded by FCT and the ERDF through COMPETE2020.

Author’s contributions

DA, RG, BS, SS and MH conceived and designed the study; DA, RG and DMH conducted the experiments; DA and RG wrote the manuscript; MH, BS and SS performed the analysis and read the paper. All authors read and approved the manuscript.

Availability of data and materials

All data are available in the main manuscript and additional file.

Ethics approval and consent to participate

Not applicable.

Consent for publication

Not applicable.

Competing interests

The authors declare no competing interests.

References

1. Sardi JCO, Scorzoni L, Bernardi T, Fusco-Almeida AM, Mendes MJS, Correspondence G, et al. *Candida* species: current epidemiology, pathogenicity, biofilm formation, natural antifungal products and new therapeutic options, J. Med. Microbiol. 2013;62:10–24.
2. Horn DL, Neofytos D, Anaissie EJ, Fishman JA, Steinbach WJ, Olyaei AJ, et al. Epidemiology and outcomes of Candidemia in 2019 patients: Data from the prospective antifungal therapy alliance registry. Clin. Infect. Dis. 2009;48:1695–1703.
3. Yapar N, Nur Y. Epidemiology and risk factors for invasive candidiasis. Ther Clin Risk Manag. 2014;10:95–105.
4. Gonçalves B, Ferreira C, Alves CT, Henriques M, Azeredo J, Silva S. Vulvovaginal candidiasis: Epidemiology, microbiology and risk factors. Crit. Rev. Microbiol. 2016;42:905–927.
5. Koehler P, Stecher M, Cornely OA, Koehler D, Vehreschild MJGT, Bohlius J, et al. Morbidity and mortality of candidaemia in Europe: an epidemiologic meta-analysis, Clin. Microbiol. Infect. 2019;25:1200-1212
6. Araújo D, Henriques M, Silva S. Portrait of *Candida* species biofilm regulatory network genes, Trends Microbiol. 2017;1:62–75.
7. Silva S, Rodrigues C, Araújo D, Rodrigues M, Henriques M. *Candida* species biofilms' antifungal resistance. J. Fungi 2017;3:8.
8. Basso V, D'Enfert C, Znaidi S, Bachellier-Bassi S. From genes to networks: The regulatory circuitry controlling *Candida albicans* morphogenesis. Curr. Top. Microbiol. Immunol. 2018;1–39.
9. Chen H, Zhou X, Ren B, Cheng L. The regulation of hyphae growth in *Candida albicans*. Virulence 2020;11:337–348.
10. Deng Y, Nong L, Huang W, Pang G, Wang Y. [Inhibition of hepatitis B virus (HBV) replication using antisense LNA targeting to both S and C genes in HBV]. Zhonghua Gan Zang Bing Za Zhi 2009;17:900–4.
11. Van Hauwermeiren F, Vandenbroucke RE, Grine L, Puimège L, Van Wonterghem E, Zhang H, et al. Antisense oligonucleotides against TNFR1 prevent toxicity of TNF/IFNγ treatment in mouse tumor models, Int. J. Cancer 2014;135:742–750.

12. Kenney SP, Meng X-J. Therapeutic targets for the treatment of hepatitis E virus infection. Expert Opin. Ther. Targets 2015;19:1245–60.
13. Warren TK, Whitehouse CA, Wells J, Welch L, Charleston JS, Heald A, et al. Delayed Time-to-Treatment of an Antisense Morpholino Oligomer Is Effective against Lethal Marburg Virus Infection. Cynomolgus Macaques, PLoS Negl. Trop. Dis. 2016;10:1–18.
14. Sully EK, Geller BL. Antisense antimicrobial therapeutics. Curr Opin Microbiol 2016;3:47–55.
15. Araújo D, Azevedo NM, Barbosa A, Almeida C, Rodrigues ME, Henriques M, et al. Application of 2'-OMethylRNA' antisense oligomer to control *Candida albicans EFG1* virulence determinant. Mol. Ther. - Nucleic Acids 2019;18:508–517.
16. Juliano RL. The delivery of therapeutic oligonucleotides. Nucleic Acids Res. 2016; 44:6518–6548.
17. Hattori Y. Progress in the development of Lipoplex and Polyplex modified with anionic polymer for efficient gene delivery. J. Genet. Med. Gene Ther. 2017;1:003–018.
18. Barba AA, Bochicchio S, Dalmoro A, Lamberti G. Lipid delivery systems for nucleic-acid-based-drugs: From production to clinical applications. Pharmaceutics 2019;11:5–7.
19. Wang Y, Miao L, Satterlee A, Huang L. Delivery of oligonucleotides with lipid nanoparticles. Adv Drug Delive Rev. 2015;87:68–80.
20. Semple SC, Akinc A, Chen J, Sandhu AP, Mui BL, Cho CK, et al. Rational design of cationic lipids for siRNA delivery. Nat. Biotechnol. 2010, 28:172–176.
21. Kranz LM, Diken M, Haas H, Kreiter S, Loquai C, Reuter KC, et al. Systemic RNA delivery to dendritic cells exploits antiviral defence for cancer immunotherapy. Nature 2016;534:396–401.
22. Safinya CR, Majzoub RN, Ewert KK. Cationic liposome-nucleic acid nanoparticle assemblies with applications in gene delivery and gene silencing. Philos. Trans. A 2016;374:20150129.
23. Akinc A, Maier MA, Manoharan M, Fitzgerald K, Jayaraman M, Barros S, et al. The Onpattro story and the clinical translation of nanomedicines containing nucleic acid-based drugs. Nature Research, 2019;14:1084-1087.
24. Gaspar R, Coelho F, Silva BFB. Lipid-nucleic acid complexes: Physicochemical aspects and prospects for cancer treatment. molecules 2020;25:5006.
25. Weisman S, Hirsch-Lerner D, Barenholz Y, Talmon Y. Nanostructure of cationic lipid-oligonucleotide complexes. Biophys. J. 2004;87:609–614.
26. Ilarduya CT, Sun Y and Düzgüneş N. Gene delivery by lipoplexes and polyplexes. 2010;40:159-70
27. Safinya CR, Ewert KK, Majzoub RN, Leal C. Cationic liposome-nucleic acid complexes for gene delivery and gene silencing. New Journal of Chemistry. 2014;38:5164-5172
28. Silva BFB, Majzoub RN, Chan C-L, Li Y, Olsson U, Safinya CR. PEGylated Cationic Liposome – DNA Complexation in brine is pathway-dependent. Biochim Biophys Acta, 2014;1838:398–412.
29. Lin AJ, Slack NL, Ahmad A, George CX, Samuel CE, Safinya CR. Three-dimensional imaging of lipid gene-carriers: Membrane charge density controls universal transfection behavior in lamellar cationic liposome-DNA complexes. Biophys. J, 2003;84:3307–3316.

30. Ahmad A, Evans HM, Ewert K, George CX, Samuel CE, Safinya CR. New multivalent cationic lipids reveal bell curve for transfection efficiency versus membrane charge density: Lipid - DNA complexes for gene delivery, J. Gene Med. 2005;7:739–748.
31. Bochicchio S, Dalmoro A, Barba A, Grassi G, Lamberti G. Liposomes as siRNA Delivery Vectors. Curr. Drug Metab. 2014;15:882–892.
32. Lin Q, Chen J, Zhang Z, Zheng G. Lipid-based nanoparticles in the systemic delivery of siRNA. Nanomedicine, 2014;9:105-20
33. Wesolowski D, Alonso D, Altman S. Combined effect of a peptide-morpholino oligonucleotide conjugate and a cell-penetrating peptide as an antibiotic, Pnas 2013;110:8686–8689.
34. Liang S, He Y, Xia Y, Wang H, Wang L, Gao R, et al. Inhibiting the growth of methicillin-resistant *Staphylococcus aureus* in vitro with antisense peptide nucleic acid conjugates targeting the ftsZ gene. Int. J. Infect. Dis. 2015;30:e1–e6.
35. Silva S, Araújo D, Azevedo NM, Almeida C, Henriques M. Antisense oligomers for controlling *Candida albicans* infections. 2020, WO 2020/174366 A1
36. Chaffin WL. *Candida albicans* cell wall proteins. Microbiol. Mol. Biol. Rev. 2008; 72:495–544.
37. Juliano RLL, Carver K. Cellular uptake and intracellular trafficking of oligonucleotides. Adv. Drug Deliv. Rev. 2015;87:35–45.
38. Young LS, Searle PF, Onion D, Mautner V. Viral gene therapy strategies: from basic science to clinical application. J. Pathol. J Pathol 2006;208:299–318.
39. Yin H, Kanasty RL, Eltoukhy AA, Vegas AJ, Dorkin JR, Anderson DG. Non-viral vectors for gene-based therapy. Nature Publishing Group, 2014;15:541-555
40. Crespo-Barreda A, Encabo-Berzosa MM, González-Pastor R, Ortíz-Teba P, Iglesias M, Serrano JL, et al. Viral and nonviral vectors for *in vivo* and *ex vivo* gene therapies. Translating Regenerative Medicine to the Clinic, 2016;155–177.
41. Merkle D, Lees-Miller SP, Cramb DT. Structure and dynamics of lipoplex formation examined using two-photon fluorescence cross-correlation spectroscopy. Biochemistry 2004;43:7263–7272.
42. Kim SA, Heinze KG, Bacia K, Waxham MN, Schwille P. Two-photon cross-correlation analysis of intracellular reactions with variable stoichiometry, Biophys. J. 2005;88:4319–4336.
43. Gómez-Varela AI, Gaspar R, Miranda A, Assis JL, Valverde RHF, Einicker-Lamas M, et al. Fluorescence cross-correlation spectroscopy as a valuable tool to characterize cationic liposome-DNA nanoparticle assembly. J. Biophotonics 2021; 14:e202000200
44. Liu X, Abbott NL. Characterization of the nanostructure of complexes formed by single-or double-stranded oligonucleotides with a cationic surfactant. J Phys Chem B. 2010;114:15554-64.
45. Rozenfeld JHK, Duarte EL, Barbosa LRS, Lamy MT. The effect of an oligonucleotide on the structure of cationic DODAB vesicles. Phys. Chem. Chem. Phys 2015;11:7498.
46. Leal C, Bouxsein NF, Ewert KK, Safinya CR. Highly efficient gene silencing activity of siRNA embedded in a nanostructured gyroid cubic lipid matrix, J. Am. Chem. Soc 2010;132:16841–16847.

47. Oliveira ACN, Martens TF, Raemdonck K, Adati RD, Feitosa E, Botelho C, et al. Dioctadecyldimethylammonium:monoolein nanocarriers for efficient in vitro gene silencing. ACS Appl. Mater. Interfaces 2014;6:6977–6989.
48. Leal C, Ewert KK, Shirazi RS, Bouxsein NF, Safinya CR. Nanogyroids incorporating multivalent lipids: Enhanced membrane charge density and pore forming ability for gene silencing. Langmuir 2011;27:7691–7697.
49. Vilela SFG, Barbosa JO, Rossoni RD, Santos JD, Prata MCA, Anbinder AL, et al. *Lactobacillus acidophilus* ATCC 4356 inhibits biofilm formation by *C. albicans* and attenuates the experimental candidiasis in *Galleria mellonella*. Virulence 2015;6:29–39.
50. Lo HJ, Köhler JR, Didomenico B, Loebenberg D, Cacciapuoti A, Fink GR. onfilamentous *C. albicans* mutants are avirulent. Cell 1997;90:939–949.
51. Torres A, Kozak J, Korolczuk A, Rycak D, Wdowiak P, Maciejewski R, et al. Locked nucleic acid-inhibitor of miR-205 decreases endometrial cancer cells proliferation *in vitro* and *in vivo*. Oncotarget 2016;7:73651–73663.
52. Kloezen W, Parel F, Brüggemann R, Brüggemann B, Asouit K, Helvert-Van Poppel M, et al. Amphotericin B and terbinafine but not the azoles prolong survival in *Galleria mellonella* larvae infected with *Madurella mycetomatis*. Med. Mycol. 2018; 56:469–478.
53. Ginn SL, Amaya AK, Abedi MR, Alexander IE, Edelstein M. Gene therapy clinical trials worldwide to 2017 : An update. J Gene Med 2018;20:e3015.
54. Bacia K, Kim SA, Schwille P. Fluorescence cross-correlation spectroscopy in living cells, Nat. Methods 2006;3:83–89.
55. Bacia K, Schwille P. Practical guidelines for dual-color fluorescence cross-correlation spectroscopy, Nat. Protoc. 2007;2:2842–2856.
56. Ries J, Petrásek Z, García-Sáez AJ, Schwille P. A comprehensive framework for fluorescence cross-correlation spectroscopy. New J. Phys. 2010;12:113009.
57. Bacia K, Haustein E, Schwille P. Fluorescence correlation spectroscopy: Principles and applications. Cold Spring Harb. Protoc. 2014;709–725.
58. Peng S, Li W, Yao Y, Xing W, Li P, Chen C. Phase separation at the nanoscale quantified by dcFCCS, Proc. Natl. Acad. Sci. 2020;117:27124-27131.
59. Ohrt T, Rg Mü Tze J, Staroske W, Weinmann L, Hö Ck J, Crell K, et al. Fluorescence correlation spectroscopy and fluorescence cross-correlation spectroscopy reveal the cytoplasmic origination of loaded nuclear RISC in vivo in human cells. Nucleic Acids Res. 2008;36:6439–6449.
60. Ohrt T, Staroske W, Rg Mü J, Crell K, Landthaler M, Schwille P. Fluorescence Cross-Correlation Spectroscopy Reveals Mechanistic Insights into the Effect of 2'-O-Methyl Modified siRNAs in Living Cells. Biophysj 2011;100:2981–2990.
61. Berezhna S, Schaefer S, Heintzmann R, Jahnz M, Boese G, Deniz A, et al. New effects in polynucleotide release from cationic lipid carriers revealed by confocal imaging, fluorescence cross-

correlation spectroscopy and single particle tracking. Biochim. Biophys. Acta - Biomembr. 2005;1669:193–207.

62. Williams DW, Wilson MJ, Lewis MAO, John A, Potts C. Identification of *Candida* species by PCR and restriction fragment length polymorphism analysis of intergenic spacer regions of ribosomal DNA. J Clin Microbiol, 1995;33:2476-9.
63. Mil-Homens D, Ferreira-Dias S, Fialho AM. Fish oils against Burkholderia and *Pseudomonas aeruginosa*: *In vitro* efficacy and their therapeutic and prophylactic effects on infected *Galleria mellonella* larvae. J. Appl. Microbiol. 2016;120:1509–1519.
64. Mil-Homens D, Bernardes N, Fialho AM. The antibacterial properties of docosahexaenoic omega-3 fatty acid against the cystic fibrosis multiresistant pathogen *Burkholderia cenocepacia*. FEMS Microbiol. Lett. 2012;328:61–69.
65. Rädler JO, Koltover I, Salditt T, Safinya CR. Structure of DNA-cationic liposome complexes: DNA intercalation in multilamellar membranes in distinct interhelical packing regimes. Science, 1997;275:810–814.
66. Koltover I, Salditt T, Rädler JO, Safinya CR. An inverted hexagonal phase of cationic liposome-DNA complexes related to DNA release and delivery, Science. 1998;281:78–81.

Figures

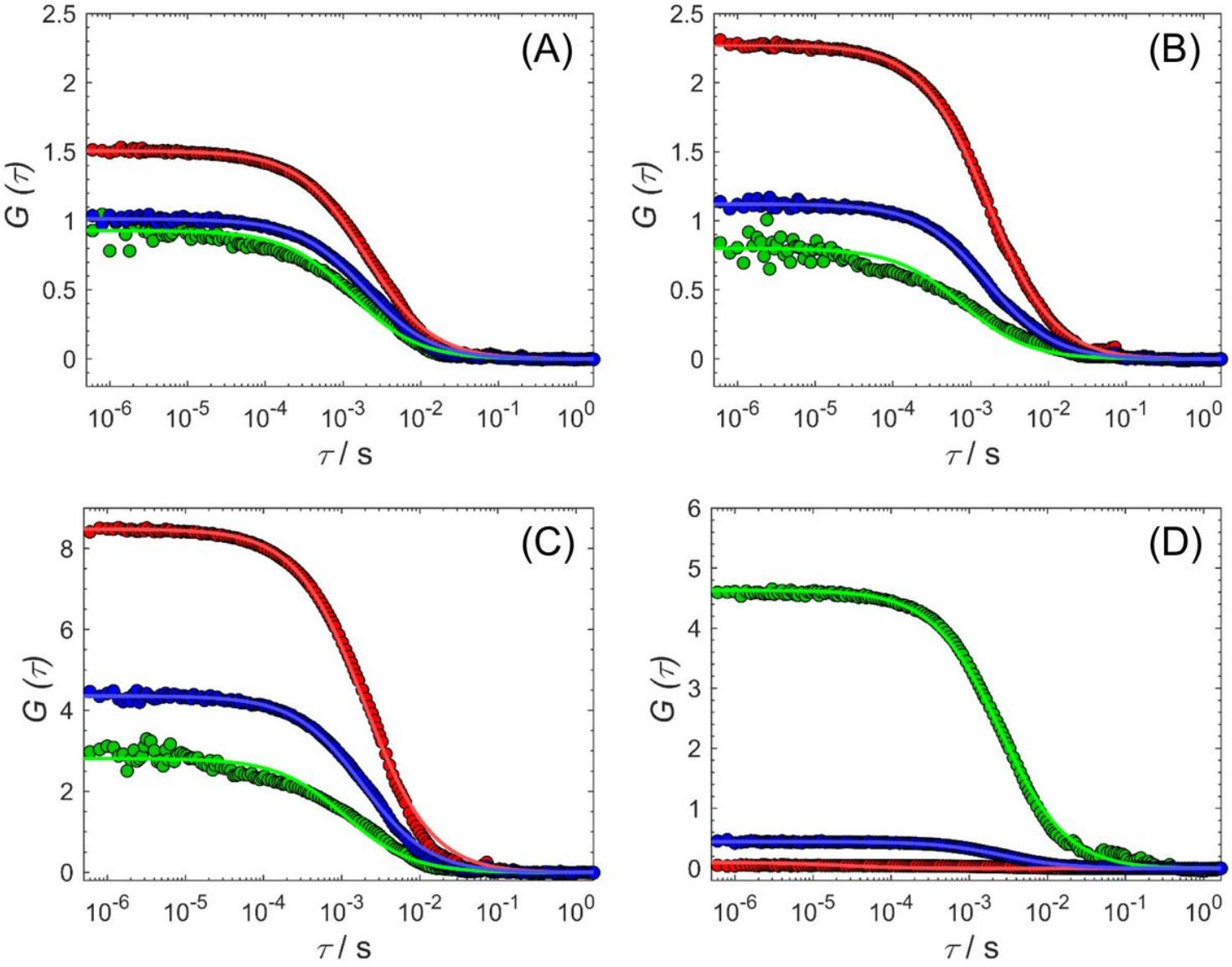

Figure 1

Fluorescence Cross-Correlation Spectroscopy data for CL-ASO of high cationic lipid content. (A) DOTAP/DOPC; (B) DOTAP/DOPE; (C) DOTAP/MO; and (D) pure DOPC formulations mixed with ASO. All cationic liposome formulations have a molar composition of 80/20 % cationic/neutral lipid and ρchg=3. The pure DOPC formulation has a total lipid amount identical to cationic liposome formulations. GG is shown in green; GR is shown in red and GX is shown in blue. The symbols represent experimental data and the lines fits to the correlation curves.

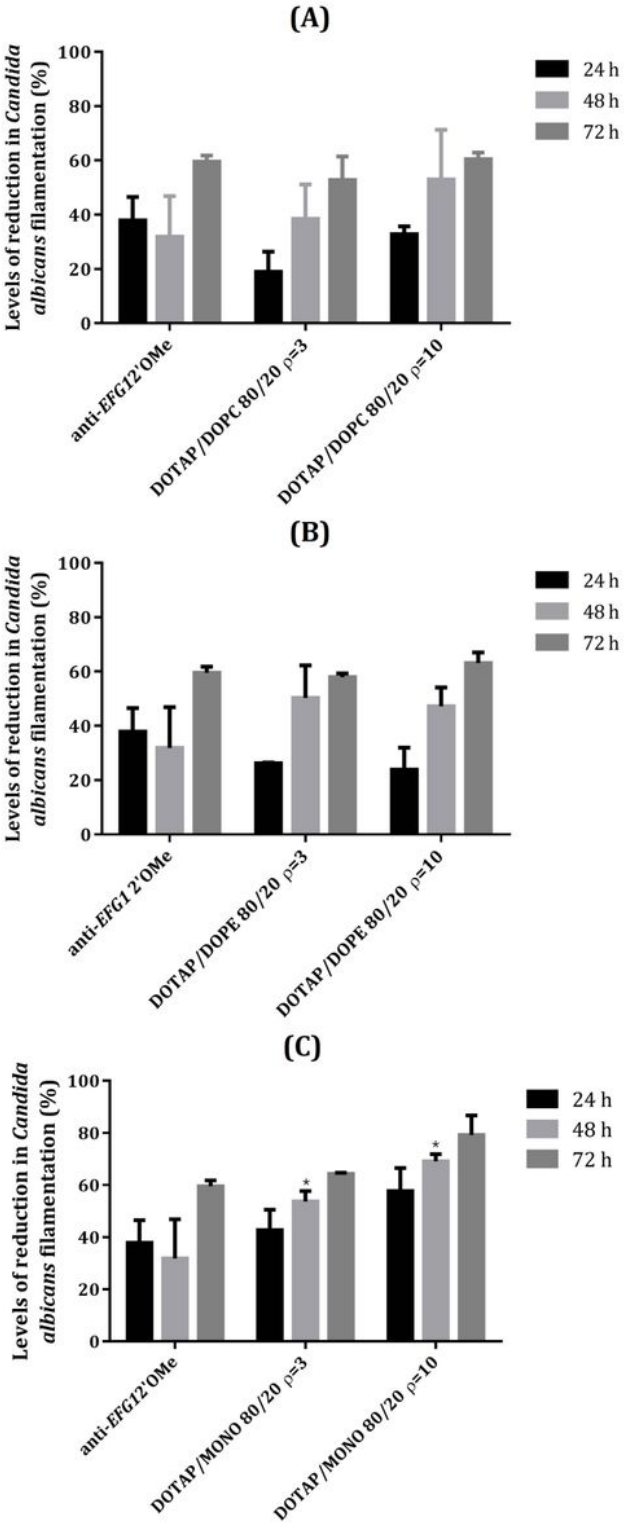

Figure 2

In vitro effect of anti-EFG1 2'OMe oligomer cationic lipid-based formulations on C. albicans filamentation. Levels of C. albicans filamentation reduction (%) of (A) DOTAP/DOPC; (B) DOTAP/DOPE and (C) DOTAP/MO after 24, 48 and 72 h of treatment with each lipoplex. As positive control, C. albicans cells were incubated in the same conditions with free anti-EFG1 2'OMe oligomer. Error bars represent standard

deviation. *Significant differences between anti-EFG1 2'OMe ASO lipid-based formulations and free ASO at each time of incubation (P-value<0.05).

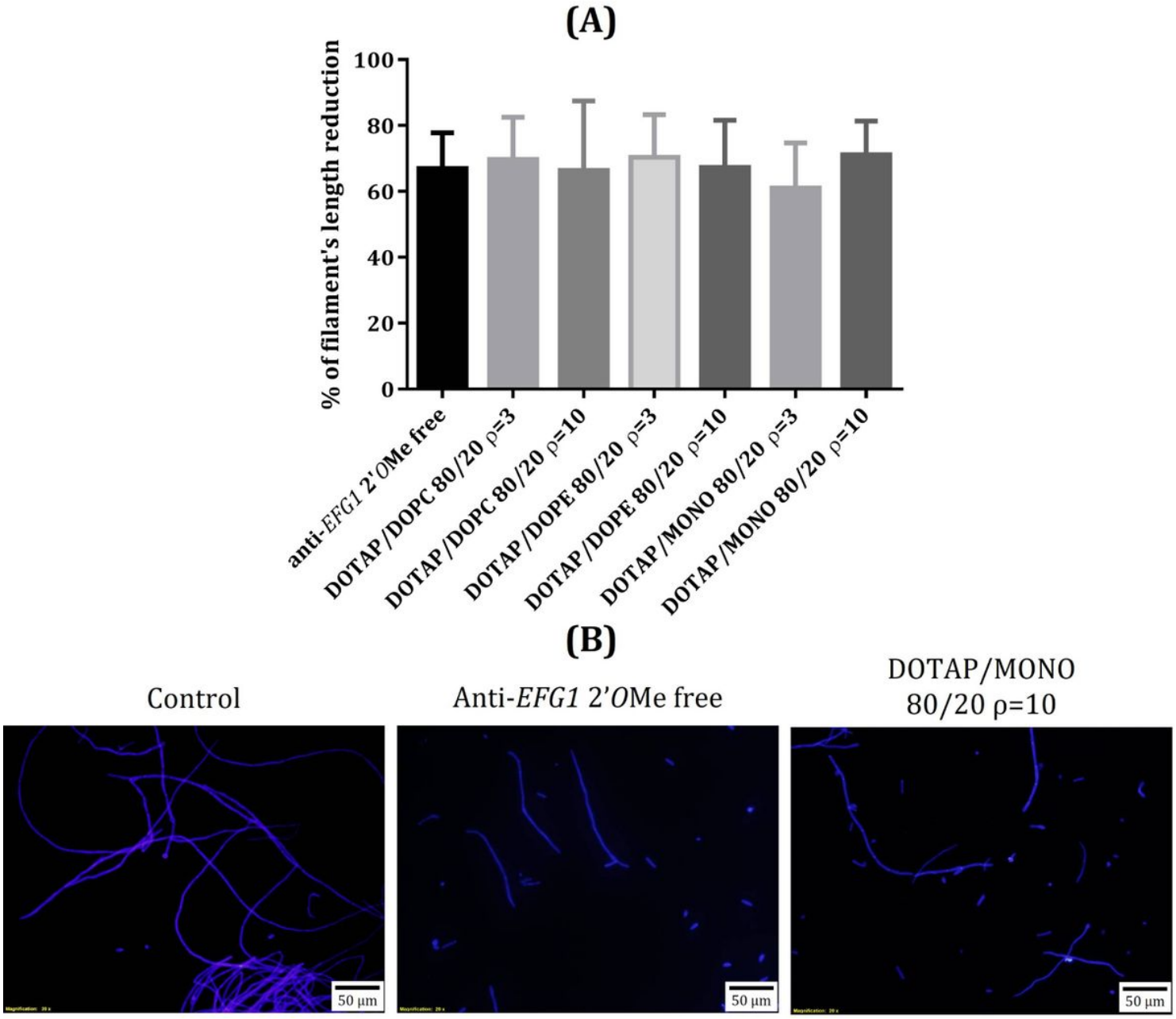

Figure 3

In vitro effect of anti-EFG1 2'OMe oligomer cationic lipid-based formulations on C. albicans filament's length. (A) Filament's length inhibition (%) determined by using ImageJ software and (B) epifluorescence microscopy images of C. albicans cells stained with calcofluor after 72 h of incubation with lipoplexes. Control represents an experiment prepared only with cells on RPMI. Anti-EFG1 2'OMe free represents the cells treated with free ASO.

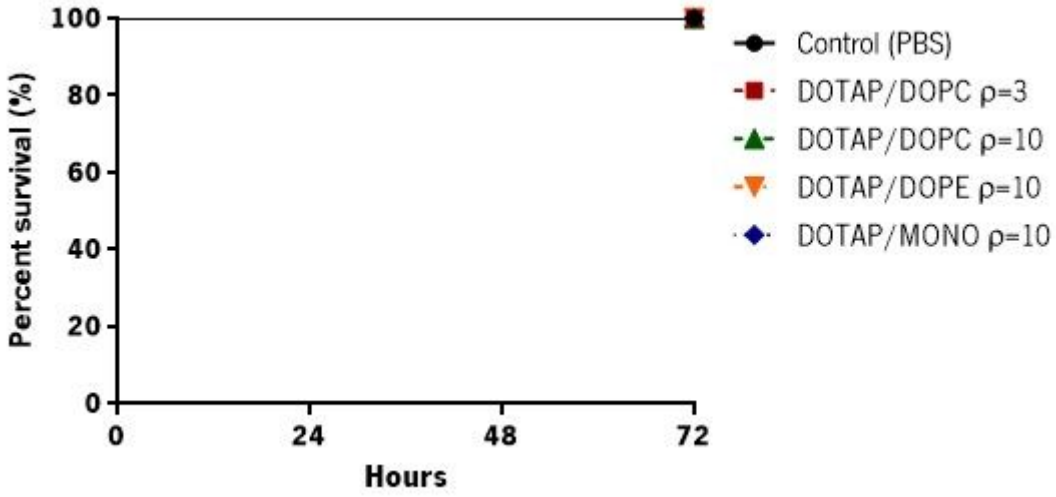

Figure 4

Anti-EFG1 2'OMe oligomer cationic lipid-based formulations toxicity evaluation on Galleria mellonella model. For each condition, 10 larvae were injected with each lipoplex, and their survival was monitored over 72 h. As control larvae were injected only with PBS.

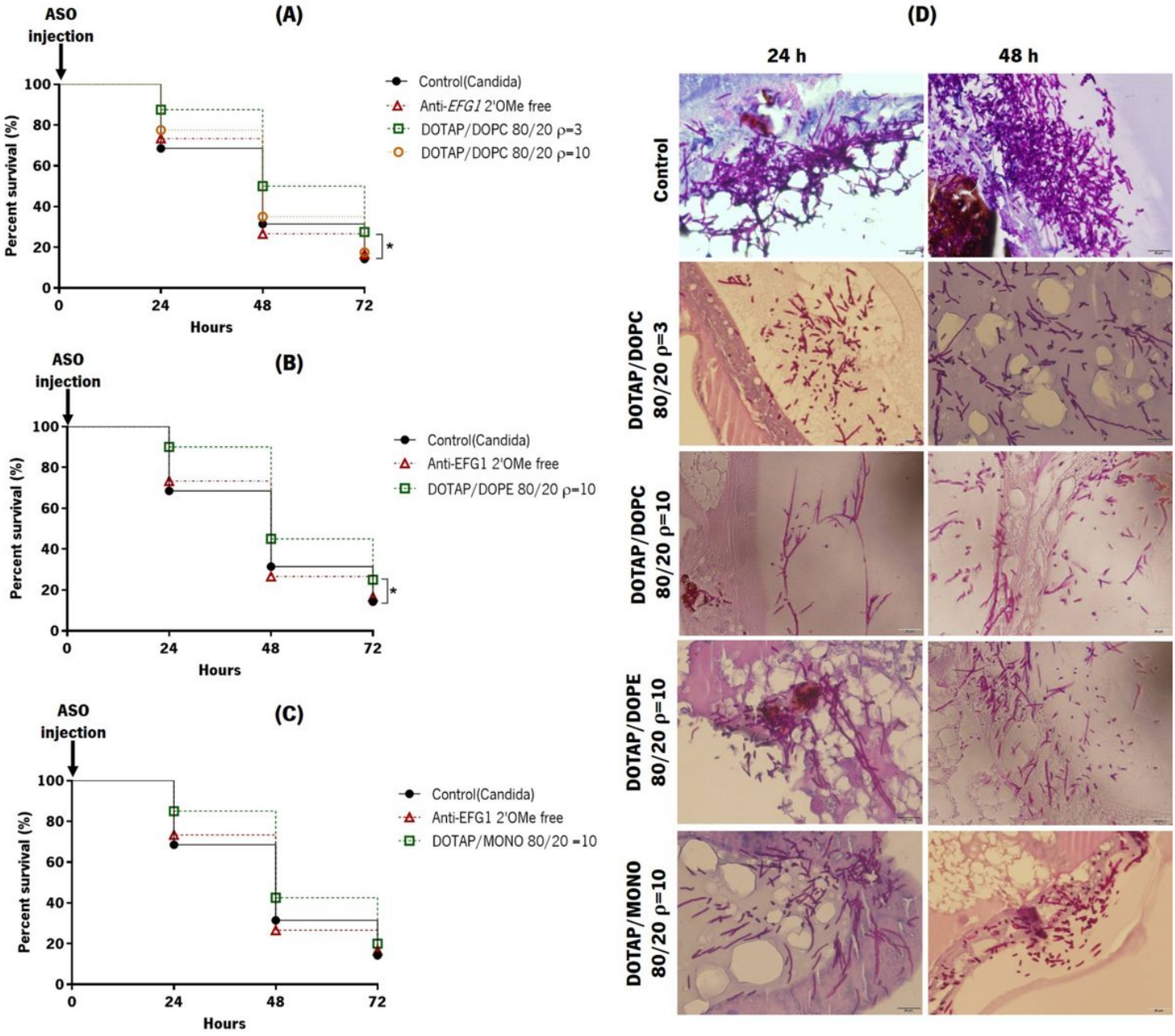

Figure 5

Single dose anti-EFG1 2'OMe oligomer cationic lipid-based formulations effect on the survival of Galleria mellonella survival infected with Candida albicans. Survival curves of infected larvae treated with a single-dose (0 h post infection) of (A) DOTAP/DOPC lipoplexes; (B) DOTAP/DOPE lipoplexes and (C) DOTAP/MO lipoplexes. (D) Histological images of the fat body of larvae infected with C. albicans and treated with a single-dose (0 h post infection) of each lipoplex at 24 h and 48 h. The larvae sections were labelled with periodic acid Schiff (PAS) coloration. The magnification images were at 400x. As control larvae infected with C. albicans cells were injected with free anti-EFG1 2'OMe ASO and only with PBS.

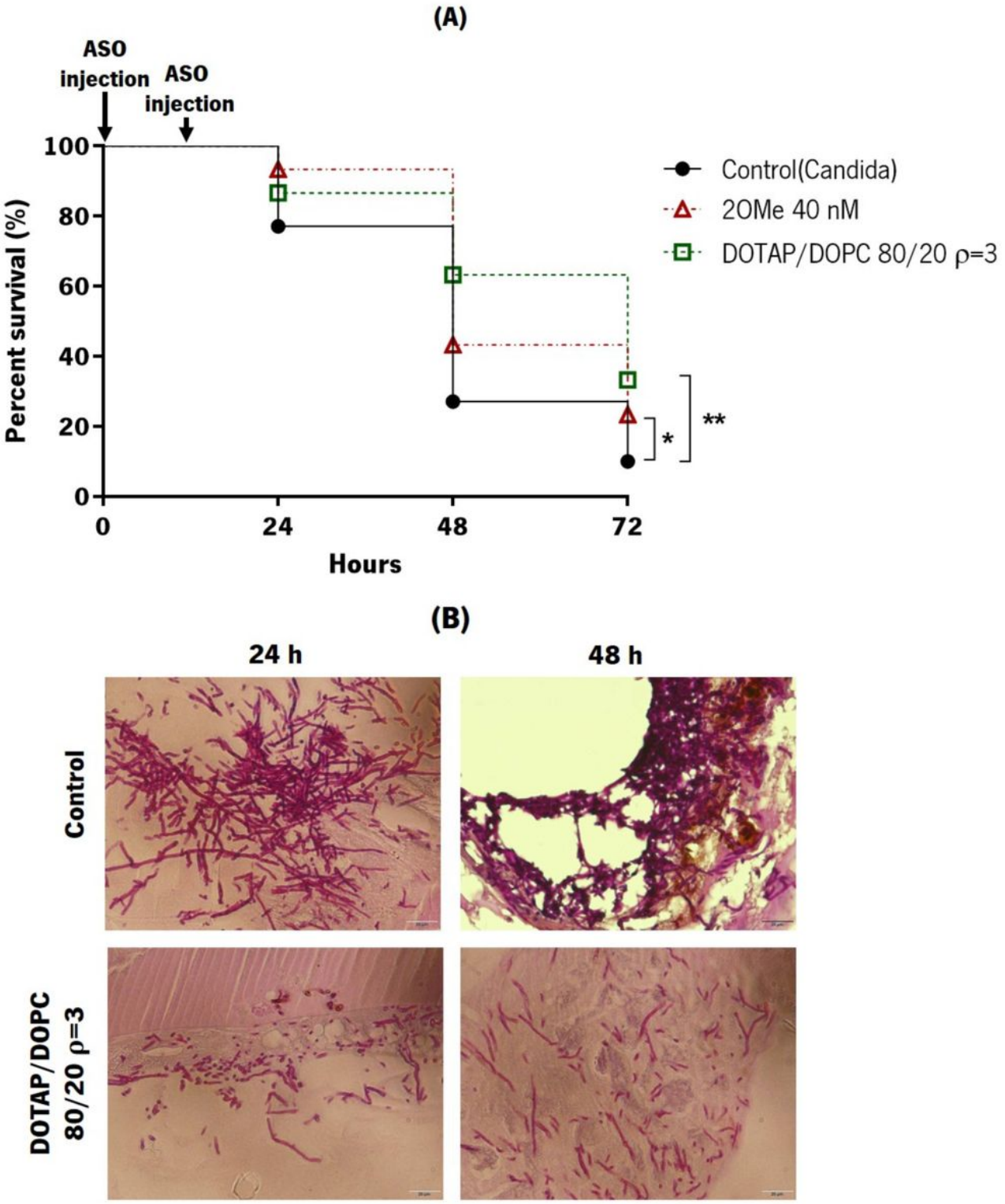

Figure 6

Double-dose anti-EFG1 2'OMe oligomer cationic lipid-based formulations effect on Galleria mellonella survival infected with Candida albicans. (A) Survival curves of infected larvae treated with a double-dose (0 h and 12 h post infection) of DOTAP/DOPC 80/20 ρchg=3 lipoplex. As control larvae infected were injected only with anti-EFG1 2'OMe free-ASO and only with PBS. (B) Histological images of larvae infected with C. albicans (at 24 h and 48 h) and treated with a double-dose (0 h and 12 h post infection)

of DOTAP/DOPC 80/20 ρchg=3 lipoplex. The larvae sections were labelled with periodic acid Schiff (PAS) coloration. The magnification images were obtained at 400x.

Supplementary Files

This is a list of supplementary files associated with this preprint. Click to download.

- SupplementalMaterial.docx
- GraphicalAbstract.jpg